Crystalline surface structures induced by ion sputtering of Al-rich icosahedral quasicrystals

Z. Shen
Ames Laboratory of the DOE and Department of Chemistry, Iowa State University, Ames, Iowa 50011

M. J. Kramer
Ames Laboratory of the DOE and Department of Materials Science and Engineering, Iowa State University, Ames, Iowa 50011

C. J. Jenks
Ames Laboratory of the DOE, Iowa State University, Ames, Iowa 50011

A. I. Goldman
Ames Laboratory of the DOE and Department of Physics and Astronomy, Iowa State University, Ames, Iowa 50011

T. Lograsso
Ames Laboratory of the DOE and Department of Materials Science and Engineering, Iowa State University, Ames, Iowa 50011

D. Delaney
Ames Laboratory of the DOE, Iowa State University, Ames, Iowa 50011

M. Heinzig
Ames Laboratory of the DOE and Department of Chemistry, Iowa State University, Ames, Iowa 50011

W. Raberg
Institut für Physikalische Chemie, Universität Bonn, Wegelerstrasse 12, 53115 Bonn, Germany

P. A. Thiel*
Ames Laboratory of the DOE and Department of Chemistry, Iowa State University, Ames, Iowa 50011

(Received 28 May 1998)

Low-energy electron diffraction patterns, produced from quasicrystal surfaces by ion sputtering and annealing to temperatures below ~700 K, can be assigned to various terminations of the cubic CsCl structure. The assignments are based upon ratios of spot spacings, estimates of surface lattice constants, bulk phase diagrams vs surface compositions, and comparisons with previous work. The CsCl overlayers are deeper than about five atomic layers, because they obscure the diffraction spots from the underlying quasicrystalline substrate. These patterns transform irreversibly to quasicrystalline(like) patterns upon annealing to higher temperatures, indicating that the cubic overlayers are metastable. Based upon the data for three chemically identical, but symmetrically inequivalent surfaces, a model is developed for the relation between the cubic overlayers and the quasicrystalline substrate. The model is based upon the related symmetries of cubic close-packed and icosahedral-packed materials. The model explains not only the symmetries of the cubic surface terminations, but also the number and orientation of domains. [S0163-1829(98)00239-2]

I. INTRODUCTION

Quasicrystals, discovered in 1982 by Shechtman and co-workers,[1,2] are typically binary and ternary metallic alloys, often containing 60–70 at. % aluminum. They present unique structural features,[3–6] coupled with unusual combinations of physical properties.[7,8] Some of the interesting properties of quasicrystals, such as low friction and ''nonstick'' character, involve surface phenomena. This motivates fundamental studies of structure, composition, and chemical reactivity of their surfaces. In many cases, one needs to separate the influence of the oxide that is always present in air, from the influence of the quasicrystalline substrate. This requires comparison of the properties of a clean surface with those of an oxidized surface, if possible.

The preparation and maintenance of a clean (nonoxidized) surface requires ultrahigh vacuum (UHV), because these Al-rich alloys oxidize readily in air. Within UHV, a convenient

route to surface preparation is ion sputtering, followed by annealing well above room temperature. Convenience is provided because a new surface can be generated repetitively on a single sample *in situ*. This approach is traditional for preparing metal samples in UHV.[9]

This method, however, can be chemically and physically disruptive. The chemical disruption is perhaps most critical for quasicrystals, since the compositional range of phase stability (in the bulk) spans only a few at. %. Indeed, some workers have suggested[10] that the evolution of the surface structure depends critically upon the local stoichiometry. Several studies, for example, have motivated a comparison, via scanning tunnel microscopy (STM) of sputtered and annealed surfaces with those prepared by *in situ* cleavage. Sputtering followed by annealing generally leads to terraced surfaces, which reveal quasiperiodic ordering of structures within and between the terraces. Those surfaces, which result from *in situ* cleaving, reveal rough terminations, on the order of cluster sizes proposed by recent structural models for the icosahedral phase.[11–13] With all of this in mind, it is clear that a deeper understanding of how chemical perturbations can force the surface out of the region of quasicrystalline stability is important for determining the true nature of the surface of quasicrystals.

The chemical changes at the surface can occur in UHV via two routes: (1) preferential sputtering of a particular metal and (2) preferential evaporation of a particular metal upon annealing. Simple momentum-transfer arguments lead to the expectation that the lightest element will be sputtered preferentially. This paper concerns the chemical perturbation and accompanying surface structures induced by the first of the two treatments, sputtering.

Schaub *et al.*[14] reported that Ar^+ sputtering of an Al-rich quasicrystal, icosahedral (*i*-) Al-Pd-Mn leads to preferential loss of Al, the lightest element. This observation has since been confirmed in other laboratories.[15–18] Similar observations—Al depletion upon Ar^+ sputtering—have been reported also on two other Al-rich alloys, *i*-Al-Cu-Fe, (Refs. 19 and 20) and decagonal Al-Ni-Co.[21]

In the bulk phase diagrams, the Al-based icosahedral alloys often have a CsCl-type structure on the Al-poor side. Rouxel *et al.* pointed out that sputtering in UHV moves the surface composition toward the region of a CsCl phase in the Al-Cu-Fe phase diagram.[19] Zurkirch, Erbudak, and Kortan observed a cubic phase induced by Ar^+ sputtering on decagonal Al-Ni-Co.[21] In a similar vein, Naumovic reported that Al depletion induced by high-temperature annealing could produce a CsCl-type structure on the fivefold surface of *i*-Al-Pd-Mn.[18,22]

These findings are all qualitatively similar to results generated within scientific communities outside of surface science. In electron microscopy, Ar^+ treatments have been reported to transform the icosahedral phase to the CsCl-type in the Al-Cu-Fe system.[23–26] In the crystal growth community, it is known that crystals with CsCl structure often coexist with the icosahedral phase.[27–30] Dong and co-workers[28,31] pointed out that it is possible to use twinning operations on the CsCl-type unit cell to describe the structure of a decagonal quasicrystal and its approximants.

In the present work, we expand upon these results with a systematic study of the crystalline overlayers produced by sputtering (followed by annealing) on four different quasicrystalline surfaces in UHV. These are all surfaces of icosahedral materials. This database allows comparisons between different high-symmetry surfaces within a single alloy, and between different alloy surfaces having the same symmetry. The three high-symmetry surfaces within a single alloy are the fivefold, threefold, and twofold surfaces of *i*-Al-Pd-Mn. The two different alloys of the same symmetry are the fivefold surfaces of *i*-Al-Pd-Mn and *i*-Al-Cu-Fe. The comparisons show that the crystalline overlayers, and their orientational relationship to the substrate, can be understood within a common general framework. This framework may prove useful for predicting and understanding the results of ion sputtering as a surface treatment on the icosahedral, Al-rich quasicrystals.

Finally, a full understanding of the properties of quasicrystals requires comparisons with the properties of crystalline samples of similar chemical composition. For purposes of surface studies in UHV, it would be especially attractive to prepare a quasicrystalline surface and a crystalline surface, from a single sample, and then to perform comparisons *in situ*. The information presented here provides the desired ability to switch between these types of surfaces, using a single bulk sample.

II. EXPERIMENTAL DESCRIPTION

The nominal compositions (i.e., the initial liquid composition used in growth) of the samples are $Al_{72}Pd_{19.5}Mn_{8.5}$ for all the Al-Pd-Mn samples, and $Al_{63}Cu_{25}Fe_{12}$ for the Al-Cu-Fe sample. Details of sample preparation and characterization, both inside and outside of UHV are given elsewhere.[32]

The low-energy electron diffraction (LEED) and Auger electron spectroscopy (AES) experiments are performed in a UHV chamber.[15] In these experiments its base pressure is $3-4\times10^{-11}$ Torr. Surface preparation in UHV involves sputtering at room temperature and annealing. The sample is sputtered for 15 min each time at normal incidence, 1 keV, and 12–18 μA sample current without bias. For a sample that has been newly mounted in UHV, annealing begins at 400 K and goes up in 50-K increments whenever annealing at a given temperature no longer reveals significant surface segregation of carbon and oxygen. The upper limits of annealing temperature are chosen to avoid phase transformations.[20] Annealing periods are typically 15–30 min during cleaning, and 1–4 h before LEED experiments. The LEED experiments are done with low-resolution optics (nominal instrumental limit 100–300 Å).

Surface compositions are monitored with electron-stimulated AES. For analyzing trends in composition, we use the Al *KLL* (1396 eV), Pd *MNN* (330 eV), Mn *LMM* (589 eV), Cu *LMM* (920 eV), and Fe *LMM* (703 eV) Auger lines. Published sensitivity factors[33] are used to calculate surface compositions. This, plus the fact that compositions are actually depth-weighted averages over regions that probably contain concentration gradients in most of these experiments (the top 100 Å), means that surface compositions should be taken as qualitative, rather than quantitative, values.

Some selected area electron diffraction (SADP) experiments are done in a transmission electron microscope

TABLE I. Auger compositions after sputtering and annealing to different temperatures. ICP-AES compositions are for samples cut from the same boule, and in most cases for a sample immediately adjacent to the one used in the UHV experiments. (a) Al-Pd-Mn twofold surface (ICP-AES composition: $Al_{71.0}Pd_{19.8}Mn_{9.2}$). (b) Al-Pd-Mn threefold surface (ICP-AES composition: $Al_{71.7}Pd_{21.8}Mn_{6.5}$). (c) Al-Pd-Mn fivefold surface (ICP-AES composition: $Al_{71.3}Pd_{19.1}Mn_{9.6}$). (d) Al-Cu-Fe fivefold surface (ICP-AES composition: $Al_{63.4}Cu_{24.0}Fe_{12.6}$).

Annealing T (K)	Al (%)	Pd (%)	Mn (%)	LEEL pattern
		(a)		
300	61±3	33±3	6±1	no pattern
600	68±2	27±2	5±2	two domains of cubic (110)
900	73±2	19±2	7±1	twofold quasicrystal
		(b)		
300	49±2	45±2	5±1	three facets
600	62	36	2	three facets + cubic (111)
800	74±1	20±2	6±1	threefold quasicrystal
		(c)		
300	52±2	43±2	5±1	no pattern
600	63±3	33±2	4±2	five domains of cubic (110)
850	71±1	23±2	6±1	fivefold quasicrystal
		(d)		
300	54±2	22±1	24±1	no pattern
600	64±1	18±1	18±1	five domains of cubic (110)
800	72±1	18±1	10±1	fivefold quasicrystal

(TEM), a Philips CM30 operated at 300 keV. The experiments were performed on a small fragment (0.1 g) of a larger ingot of i-$Al_{65}Cu_{23}Fe_{12}$. The piece was ground in ethanol, and a droplet of the suspension was dried in air onto a continuous carbon film supported by a 300-mesh Cu grid. Care was taken so the particles were not in contact with the Cu mesh. The grid was then placed between Pt spacers in a Gatan double tilt TEM stage with resistive heating, and with a Pt/Pt-Rh thermocouple to monitor the temperature. Exact temperature is uncertain due to poor thermal contact, and in the heating experiments a temperature lag of 100 K is not unusual. A thin area of a single grain was obtained for SADP and the grain was tilted to a fivefold zone axis. Heating was performed incrementally, with SADP's taken approximately every 50 K for temperatures up to 1070 K.

III. RESULTS

Surface compositions after Ar^+ sputtering and annealing at different temperatures are shown in Table I. It can be seen that the surfaces are all Al deficient, relative to the nominal bulk composition, after sputtering at room temperature. The Al-Pd-Mn surfaces are all Pd rich, and the Al-Cu-Fe surface is Fe rich (relative to the bulk). Heating to 800–900 K in all cases restores the surface to a composition close to that of the bulk.

Ar^+ sputtering and annealing in UHV yields two different types of LEED patterns for all four samples (Fig. 1). The first is obtained upon annealing at relatively low temperature: 600–800 K for the Al-Pd-Mn twofold surface [Fig. 1(a)], 300–650 K for the Al-Pd-Mn threefold surface [Fig. 1(b)], 600–750 K for the Al-Pd-Mn fivefold surface [Fig. 1(c)], and 500–750 K for the Al-Cu-Fe fivefold surface [Fig. 1(d)]. The second is obtained after annealing at higher temperature: 800–900 K for the Al-Pd-Mn twofold surface [Fig. 1(e)], 650–800 K for the Al-Pd-Mn threefold surface [Fig. 1(f)], 700–800 K for the Al-Pd-Mn fivefold surface [Fig. 1(g)], and 750–850 K for the Al-Cu-Fe fivefold surface [Fig. 1(h)].

A. Assignment of the high-temperature patterns

The high-temperature LEED patterns have very sharp LEED spots, as can be seen in the right-hand column of Fig. 1. The widths of the spots correspond to a real-space dimension greater than 150 Å in width, and are limited by the LEED optics. A further high-resolution LEED study on the Al-Pd-Mn fivefold surface shows that the average domain size is about 900 Å (again, close to the resolution limit of the LEED instrument). The existence of large terraces, with average lengths in the range of hundreds of Å, is also supported by atomic force microscopy on the Al-Pd-Mn threefold[34] and twofold[35] surfaces. The symmetries and spot spacings in the

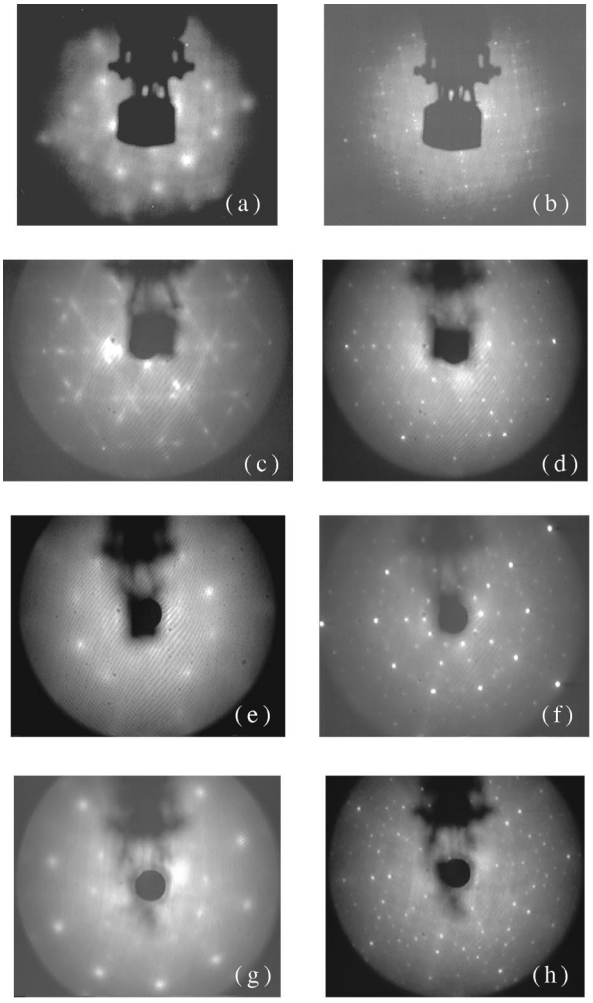

FIG. 1. LEED patterns at normal incidence. (a) Pseudotwofold pattern of Al-Pd-Mn twofold surface obtained by annealing at 600 K for 3.5 h, $E=110$ eV; (b) twofold pattern of Al-Pd-Mn twofold surface obtained by annealing at 900 K for 4 h, $E=110$ eV; (c) pseudothreefold pattern of Al-Pd-Mn threefold surface obtained by annealing at 650 K for 1 h; (d) threefold pattern of Al-Pd-Mn threefold surface obtained by annealing at 700 K for 1 h; $E=60$ eV; (e) pseudotenfold pattern of Al-Pd-Mn fivefold surface obtained by annealing at 650 K for 0.5 h, $E=50$ eV; (f) fivefold pattern of Al-Pd-Mn fivefold surface obtained by annealing at 800 K for 2 h, $E=50$ eV; (g) pseudotenfold pattern of Al-Cu-Fe fivefold surface obtained by annealing at 500 K for 0.5 h, $E=150$ eV; (h) fivefold pattern of Al-Cu-Fe fivefold surface obtained by annealing at 850 K for 1 h, $E=150$ eV.

high-temperature LEED patterns correspond well to those expected for unreconstructed quasicrystalline surfaces.[36] Thus, the data are consistent with unreconstructed quasicrystalline surfaces, or, perhaps, with high-order approximants, such as suggested by Dubois.[8]

Turning now to the LEED patterns obtained after the low-temperature anneal, we note that the diffraction spots are quite broad (see Fig. 1), and the patterns do not correspond to those expected for bulk-terminated icosahedral quasicrystalline surfaces. However, the symmetries of the LEED patterns have an apparent relationship to the underlying bulk structure: twofold LEED pattern for the twofold termination, threefold LEED pattern for threefold termination, and tenfold LEED patterns for fivefold terminations. The nature of the low-temperature patterns is discussed later in this paper.

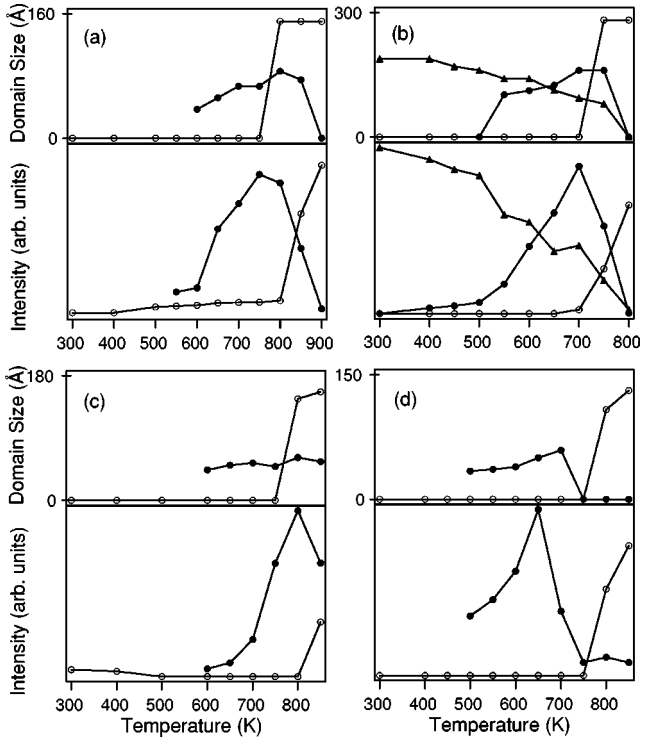

FIG. 2. Temperature-dependence of the LEED intensities and domain size for the low-temperature patterns (solid circles) and high-temperature patterns (open circles). (a) Al-Pd-Mn twofold surface; (b) Al-Pd-Mn threefold surface (solid triangles are the first crystalline phase after sputtering); (c) Al-Pd-Mn fivefold surface; (d) Al-Cu-Fe fivefold surface. These intensities were all measured at 120 K after heating to the temperature indicated.

B. Transitions between low- and high-temperature structures

In order to study the evolution of the low- and high-temperature LEED patterns, we monitored the intensities and widths of diffraction spots of both the patterns as a function of temperature while heating the sample at a rate of 0.1 K/sec. The results, shown in Fig. 2, indicate that there is a rather abrupt transition from the low-temperature to high-temperature phase. The transition temperature is around 800 K for the twofold Al-Pd-Mn surface, 750 K for the threefold surface of Al-Pd-Mn, 800 K for the fivefold Al-Pd-Mn surface, and 800 K for the fivefold surface of Al-Cu-Fe. These transitions are irreversible based upon the observation that the data of Fig. 2 remain unchanged (expect for variations ascribable to Debye-Waller effects) when the data are acquired at $T=120$ K after each annealing step, or are acquired at the annealing temperature directly. The data of Fig. 2 were acquired under the former conditions.

C. Degeneracies in the low-temperature patterns

By examining LEED patterns at different places on the samples, we found that the low-temperature LEED patterns actually consist of multiple rotational domains for fivefold and twofold surfaces: five domains for fivefold surfaces, and two domains for the twofold surface. The degeneracy of the

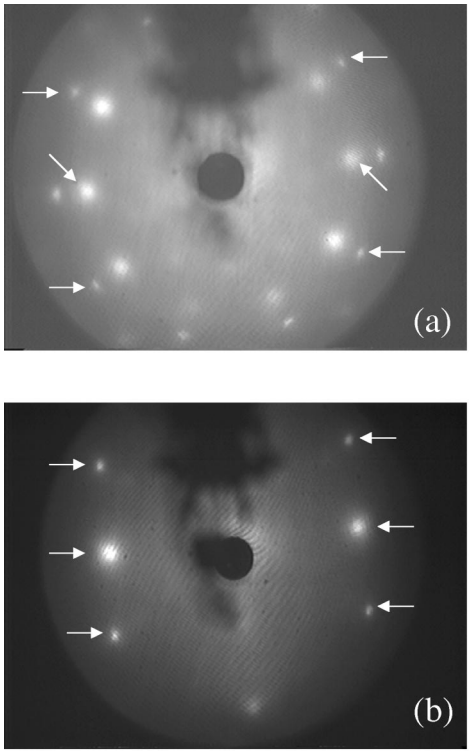

FIG. 3. (a) Pseudotenfold LEED pattern of Al-Cu-Fe obtained after annealing at 500 K for 0.5 h, $E=70$ eV; (b) single domain LEED pattern obtained by annealing at 550 K for 2 h.

multiple domains is broken in certain spots of the sample, mainly near the edges. This is observed most clearly for the Al-Cu-Fe fivefold surface (Fig. 3). The apparent tenfold pattern [Fig. 3(a)] actually consists of five rotational domains [Fig. 3(b)], which are separated by 72° from each other. The pattern has been called previously[20,37] the *pseudotenfold* pattern. The interpretation is the same for the low-temperature LEED pattern of fivefold Al-Pd-Mn.

As a check, we measured the intensity-voltage (I-V) curves of LEED spots in the tenfold patterns, both of Al-Cu-Fe [Fig. 3(a)] and Al-Pd-Mn. For spots that were equidistant from the specular beam, the intensity-voltage curves were equivalent. This is expected for overlapping domains.

For the Al-Pd-Mn twofold surface, the two domains can be described as symmetric about the two icosahedral twofold axes in the twofold plane (Fig. 4). It is interesting that there is an angle of about 34° between the single domain edge and one of the two twofold axes [Fig. 4(b)]. We offer an explanation of this angle later in the paper.

Things are more complicated for the threefold surface. There are actually two sets of LEED patterns in Fig. 1(c). The first is obtained just after sputtering at room temperature, with no annealing [Fig. 5(a)]. The diffraction spots are relatively sharp and the pattern has apparent threefold symmetry. This pattern also contains multiple (three) domains [Fig. 5(b)]. These three domains are separated by 120°. Interestingly, the orientations of the single domains deviate slightly (by a few degrees) from the average surface orientation. Thus, they are actually facets on the surface, which is why some of the diffraction spots appear to be split in Fig. 1(c). The intensity of this low-temperature pattern—which

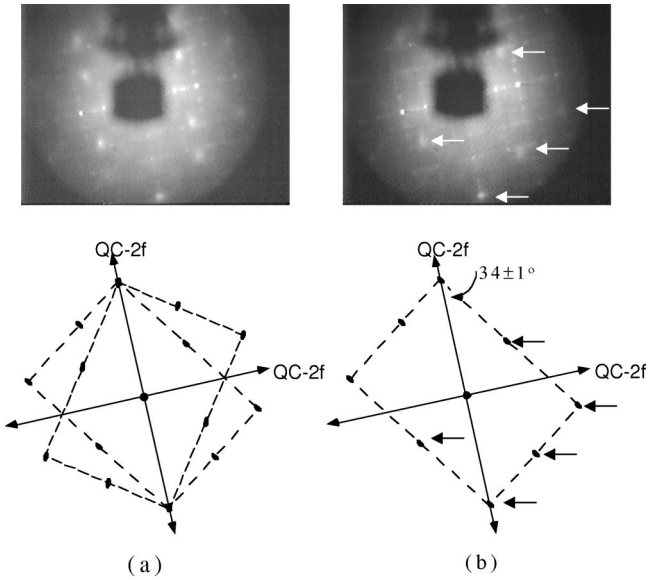

FIG. 4. LEED patterns and schematic drawing of Al-Pd-Mn twofold surface after sputtering and annealing at 750 K for 5 hours, $E=60$ eV. Both cubic and quasicrystal patterns are present. (a) Two domains of cubic phase; (b) one domain of cubic phase.

we call the facetted pattern—decreases as annealing temperature increases [Fig. 2(b), solid triangles].

The second low-temperature pattern appears after annealing between 550 and 700 K [solid circles, Fig. 2(b)], and before the facetted pattern disappears. The diffraction spots are slightly broader than the first pattern. This pattern has threefold symmetry too, but is distinguished by the streaks shown in Fig. 1(c). All attempts to find areas of broken degeneracy at different locations on the crystal failed. However, the distinctive streaks in this pattern suggest that a domain structure is present, although its exact nature is not known at this time.

D. Assignment of the low-temperature patterns

Surprisingly, the single domain LEED patterns for the twofold and fivefold surfaces are very similar. They share the same geometry and spacing. We concentrate on the Al-Cu-Fe fivefold surface first in the following discussion.

The single domain LEED pattern [Fig. 3(b)] is periodic, which indicates that the corresponding surface structure is crystalline. The ratio between the two edges of the rectangle is 1.41 ± 0.02. This suggests that the surface structure is probably cubic with (110) orientation, for which the theoretical edge ratio is $\sqrt{2}=1.414$.

The cubic CsCl structure in the Al-Cu-Fe system is called the β phase. Its general stoichiometry is denoted $Al(Cu_{1-x}Fe_x)$, and it is stable in the bulk for Fe concentrations in the range 10–50 % and Cu concentration in the range 0–40 %.[38]

One way to check the identification of the CsCl structure is by estimating the absolute lattice constant *within the surface plane* from the LEED patterns. The uncertainty in such a measurement is large, mainly because of uncertainty about whether the sample is close to the focal point of the optics. We attempted to compensate for this uncertainty by scaling the LEED value to that determined for the quasicrystalline

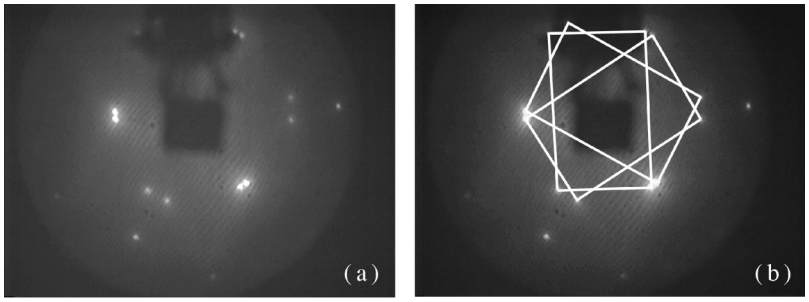

FIG. 5. (a) LEED pattern of Al-Pd-Mn threefold surface just after sputtering; (b) with schematic drawing of three domains (or facets), $E=45$ eV.

surface, and assuming that the quasicrystalline surface has the same quasilattice constant as the quasicrystalline bulk. The result for the pseudotenfold pattern is 2.95 ± 0.05 Å. The bulk lattice constant of β-AlFe [i.e., $x=1$ in β-Al($Cu_{1-x}Fe_x$)] is 2.902–2.908 Å.[39] However, our β phase probably contains significant Cu [Table I(d)], which might influence the bulk lattice constant. X-ray diffraction data from a hot-isostatically-pressed sample of the β phase with bulk composition $Al_{50}Cu_{35}Fe_{15}$ indicates a higher bulk lattice constant of $2.9422(4)\pm0.0004$ Å, i.e., an expansion of 0.03–0.04 Å relative to the composition with no Cu. This is closer to the value measured from LEED.

The lattice constant *perpendicular* to the surface of the crystalline overlayer can also be determined by a measurement of the step heights in LEED. This relies upon determining the electron wavelengths at which scattering from successive terraces is in phase or out of phase.[40,41] The measurement is suggested by the data of Fig. 3(b), which show that some diffraction spots are sharp (scattering is in phase), while others are broad (out of phase), at the particular electron energy (electron wavelength) of 70 eV. This relationship between the different diffraction spots is a consequence of the arrangement of scatterers in successive terraces.[40,41] A measurement of spot widths vs electron energy is shown in Fig. 6. The separation between successive maxima or minima corresponds to the average step height. It can be seen that the step height from this measurement is in the range of 2.2–2.3 Å. The separation between successive (110)-type planes in the bulk CsCl structure of Al-Cu-Fe

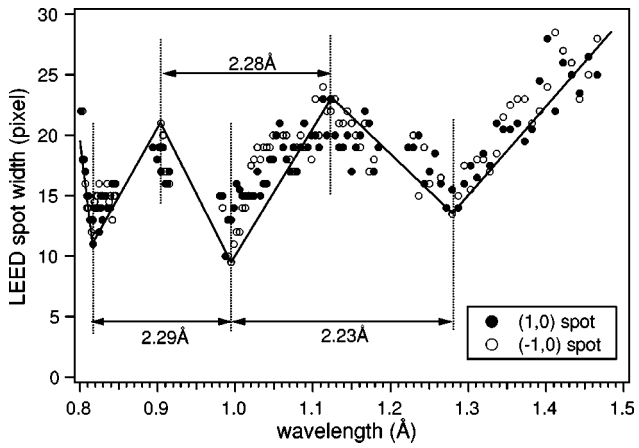

FIG. 6. Widths of two symmetry-equivalent LEED spots, as a function of electron wavelength. Minima correspond to out-of-phase scattering, and maxima correspond to in-phase scattering.

should be 2.05–2.08 Å, somewhat smaller than the data indicate. The discrepancy may be due to some step bunching, which would increase the average experimental value. (Note that surface relaxations should not play a part in the comparison between expected and measured values, assuming that such relaxations affect all terraces equally.)

Auger compositions [Table I(d)] show that Ar^+ sputtering at room temperature serves to deplete the Al and enrich the Fe. As pointed out previously by Rouxel *et al.*,[19] sputtering moves the surface composition in the direction of the β phase. There are several reasons why the measured compositions may not correspond more closely to the 50 at. % Al content expected for the bulk. These include uncertainties in the accuracy of the Auger measurement (Sec. II), the probability that Auger probes both the quasicrystalline substrate and the β overlayer (Sec. II), and the high density of domain boundaries within the β phase.[31]

Analysis of LEED intensity-voltage data has been done on the single-domain LEED pattern of the fivefold Al-Cu-Fe surface.[37] The analysis gives preference to a pure unreconstructed β-Al($Cu_{1-x}Fe_x$) (110) surface with a copper-rich composition. The best Pendry R factor is 0.262, which is considered an acceptable value.

All these results suggest that the low-temperature phase is probably β-Al($Cu_{1-x}Fe_x$) with (110) surface orientation. There is an orientational relationship between the β phase and the underlying quasicrystalline phase.

Similar discussion can be applied to the Al-Pd-Mn quasicrystals. There is a crystalline β-AlPd phase with CsCl structure and a lattice constant of 3.04–3.06 Å.[39] The lattice constant after partial substitution of Mn for Pd, β-$Al_{48}Pd_{10}Mn_{42}$, is slightly lower: 3.02 Å.[42] The symmetries of the low-temperature single domain LEED patterns of Al-Pd-Mn twofold, threefold, and fivefold surfaces correspond well to expectations for cubic (110), (111), and (110) surfaces, respectively. The lattice constants determined from the LEED patterns are 2.95 ± 0.1 Å for the twofold surface, 3.03 ± 0.1 Å for the threefold surface (the streaked pattern), and 2.94 ± 0.1 Å for the fivefold surface. The ratios of edges of single domain LEED patterns are 1.42 ± 0.02 for the twofold surface and 1.42 ± 0.02 for the fivefold surface. Auger compositions [Tables I(a)–I(c)] of these three surfaces after Ar^+ sputtering are also in the direction of the β-phase.

All these results suggest that a cubic Al($Pd_{1-x}Mn_x$) phase forms on the Al-Pd-Mn surfaces after Ar^+ sputtering and mild annealing (to below ~700 K). The surface orientation of this cubic phase is related to the underlying quasicrystal-

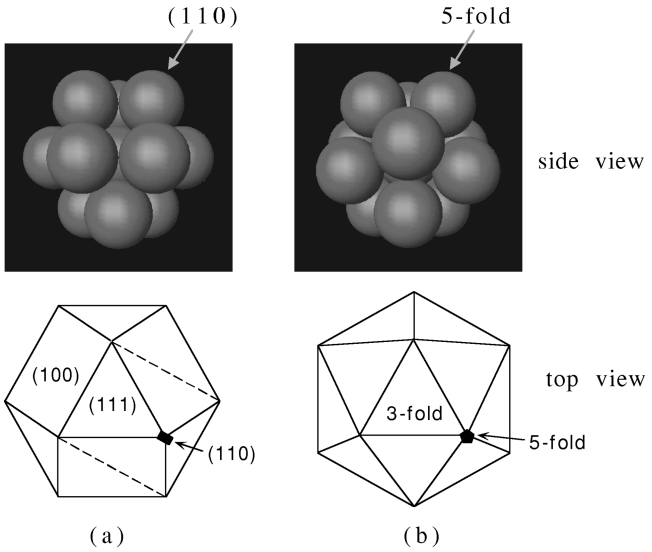

FIG. 7. Structure models of (a) cubic close packed (ccp) cluster; (b) icosahedral packed (ip) cluster. Top row is side view, and bottom row is top view.

line surface structure. Cubic (110) surfaces are formed on the twofold and fivefold quasicrystal surfaces, and a cubic (111) surface is formed on the threefold quasicrystal surface. After high-temperature annealing (above ~700 K), this cubic phase transforms to the quasicrystal.

Note that this discussion does not encompass the facetted pattern on the threefold surface. The average ratio of the edges of the rectangles in Fig. 5(b) is 1.59, so this is not a ''simple'' (110) termination. The nature of this pattern is not known at present.

The present work serves as a revision to a previous report that the low-temperature phase on twofold *i*-Al-Pd-Mn had icosahedral, or near-icosahedral, symmetry; in that work, the degeneracy of the LEED pattern was not yet identified.[43]

E. Structural relationship of the low-temperature phases to the quasicrystalline substrate

Obviously, the quasicrystalline substrate exerts a strong influence on the orientation and surface termination of the crystalline overlayer. As a starting point to discuss this relationship, let us take a very simple structural model: packing of equal spheres. In the cubic close-packing (ccp) of equal spheres [Fig. 7(a)] each sphere is surrounded by 12 nearest neighbors, and there are 4 threefold axes, 6 twofold axes, and 4 fourfold axes in the cubic structure. In the icosahedral packing (ip) of equal spheres [Fig. 7(b)], each sphere also has 12 nearest neighbors, and there are 15 twofold axes, 10 threefold axes, and 6 fivefold axes.

The difference between these two dense packings is mainly in the middle layer: in icosahedral packing it is buckled instead of planar as in ccp, and it is rotated by 30° compared to ccp (Fig. 7 top). So if one starts from a ccp cluster, then rotates the middle six spheres by 30°, displaces three of them up by about 20% and the other three down by about 20% of the interatomic distance, one gets icosahedral packing. The total displacement of the spheres is about 50% of the interatomic distance for the middle six spheres and about 4% for the top and bottom six spheres.

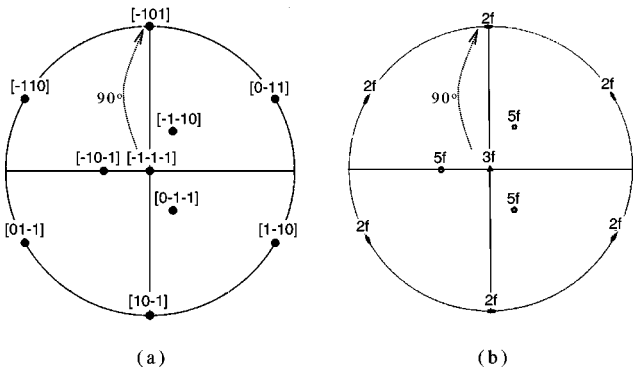

FIG. 8. Stereographic projection of (a) cubic [111] zone axis; (b) icosahedral threefold zone axis. The azimuthal relationship between the two projections is that proposed in this paper. The high-symmetry axes that are parallel, or nearly so, in the two structures are labeled.

Based upon this transformation, there is a close relationship between the symmetry axes of these two types of packing. This can be shown more clearly in stereographic projections. Since the threefold axis is common in the ccp and ip symmetries, that is the starting point. Figure 8 is a comparison of the ccp (111) projection and the ip threefold projection. The three [110]-type axes of ccp that are perpendicular to the [111] axis are lined up with the three twofold axes of ip. The other three [110]-type axes of ccp that are 35.26° away from the [111] axis are almost parallel to three fivefold axes of ip (2.1° off).

The experimental data for the twofold Al-Pd-Mn surface show that the two domains of the cubic phase are symmetric about the two icosahedral twofold axes in the twofold plane (Fig. 4). This can be explained by the twofold stereographic projection of the icosahedral surface [Fig. 9(a)], where there are two twofold axes and two threefold axes in the plane that are perpendicular to the surface normal. According to our model, there are two possible domains of the cubic phase that can grow on the quasicrystal twofold surface: the [111] directions of these two domains are parallel to the two threefold axes that are perpendicular to the surface normal. From Fig. 9(a), it is easy to see that these two domains are symmetric about the two icosahedral twofold axes in the plane.

The angle of 34° between the edge of the cubic, single-domain LEED pattern and one of the twofold axes in the quasicrystal LEED pattern [Fig. 4(b)] can also be explained.

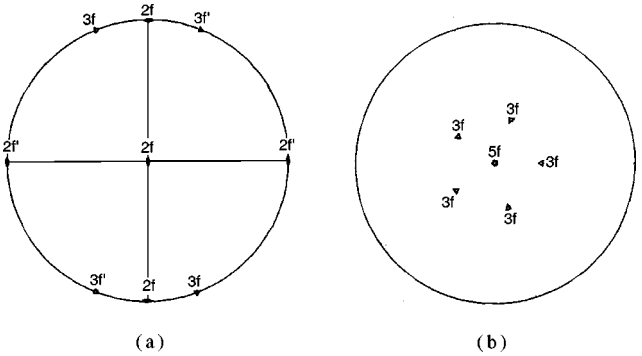

FIG. 9. Stereographic projection of icosahedral (a) twofold surface; (b) fivefold surface.

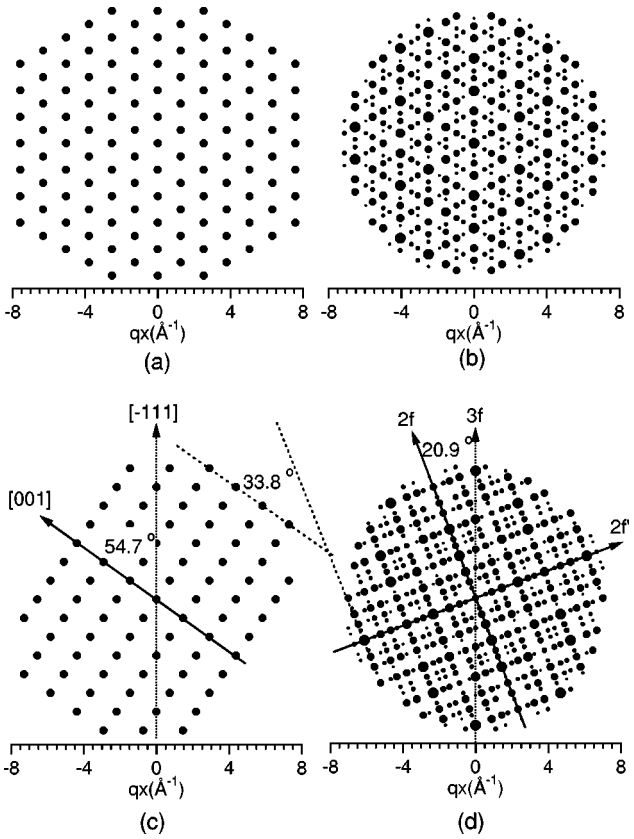

FIG. 10. Simulated LEED patterns of (a) cubic (111) surface; (b) icosahedral threefold surface; (c) cubic (110) surface; (d) icosahedral twofold surface.

The angle between the ip threefold and twofold axes [labeled $3f$ and $2f$, respectively, in the twofold projection of Fig. 9(a)] is 20.9°. The angle between a threefold axis and a [001]-type axis in the ccp twofold projection (not shown) is 54.7°. The [001] axis is parallel to the edge of the rectangular unit cell indicated in Fig. 4(b). This implies that the angle between the ip twofold axis and the ccp [001]-type axis is $54.7° - 20.9° = 33.8°$, in quantitative agreement with the experiment.

As a check, let us examine the LEED patterns of the twofold surface in this context. Again, we start from the threefold surface because, according to our model, the ccp (111) surface and ip threefold surfaces should be aligned to each other. So we align the simulated LEED patterns of ccp (111) and ip threefold surfaces to each other [Figs. 10(a) and 10(b)]. Then we rotate both the cubic (111) surface and icosahedral threefold surface 90° to one of the three cubic (110)-type or icosahedral twofold surfaces (following the dashed arrows in Fig. 8). The simulated LEED patterns after the rotation are shown in Figs. 10(c) and 10(d). The angle between the cubic [001] direction and one of the icosahedral twofold axes is 33.8°. To get the other domain, one would start from a different threefold axis, and rotate into the same twofold axis.

Similar discussion can be applied to fivefold surfaces. Figure 9(b) shows there are five possible growth directions (along five icosahedral threefold axes) for the cubic phase on the fivefold quasicrystal surface, which generates five cubic (110) domains on the surface.

We conclude that there is a close structure relationship between cubic close packing and icosahedral packing, and that this controls the growth orientation in our experiments. The key relationships between ccp and ip are [110] of ccp ∥ twofold of ip, [110] of ccp almost ∥ fivefold of ip, and [111] of ccp ∥ threefold of ip.

Table II compares these LEED results with previous electron microscopy and high-energy electron diffraction studies. For the twofold icosahedral axis, the relationship [110] of CsCl ∥ twofold of ip, is observed. Two additional observations, [112] or [111] ∥ twofold, can be rationalized on the basis that the [112]- and [111]-type axes are only 1.44°–1.45° away from the remaining twofolds of ip, based on our model. For the fivefold and threefold icosahedral axes, the relationship [110] ∥ fivefold seems robust. The additional observation of [113] ∥ fivefold can be rationalized similarly: the [113]-type axis is within 0.8° of three of the fivefolds of ip, in our model. In comparing the experimental data of Fig. 2, note that our experiments measure only the orientation of the axes that are parallel to the surface plane. Electron microscopy techniques also probe axes that are not parallel to the surface, due to the ease of sample rotation and higher penetration depth of the electrons. (Other differences also exist, which complicate the comparison between LEED and electron microscopy techniques.[44]) A general observation from our experiments is that the system selects surface planes that maximize the alignment between high-symmetry axes of substrate and overlayer. This explains, for instance, why the surface of the cubic layer on the twofold surface is not (112) or (111), which would incur a misalignment of 1.44°–1.45°, but rather (110).

SADP's of an $Al_{65}Cu_{23}Fe_{12}$ single grain in our laboratory also support one of these relationships (Fig. 11). In the

TABLE II. Observed relations between symmetry axes in icosahedral and CsCl-type systems. Results from different groups are listed separately. Note that the present work differs from the others in that it only probes axes that are parallel to the sample surface (or, equivalently, to the icosahedral-CsCl interface).

Icosahedral axis	Parallel CsCl axis type in Fe-Ti (Refs. 29 and 30)	Parallel CsCl axis type in Al-Cu-Fe (Ref. 27)	Parallel CsCl axis type in Al-Cu-Fe (Ref. 23)	Parallel CsCl axis type in Al-Cu-Fe (Refs. 24–26)	Parallel CsCl axis type in Al-Pd-Mn and Al-Cu-Fe (present work)
$2f$	[110] or [112]	[110] or [111]	[110] or [111]	[111]	[110]
$5f$	[110]	[110] or [113]	[110]	[110] or [113]	[110]
$3f$	[111]		[111]		[111]

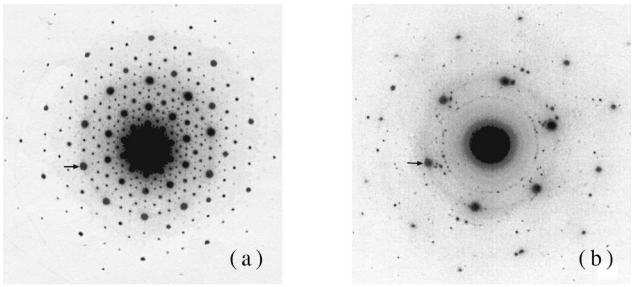

FIG. 11. SADP patterns of an *i*-Al-Cu-Fe single grain (a) at room temperature, and (b) after heating to 970 K. The arrow in (a) denotes a (110)-type reflection, and in (b) it denotes one of the icosahedral twofold reflections.

SADP experiment, an icosahedral grain was oriented to a fivefold zone axis [Fig. 11(a)], and was heated until peritectic decomposition yielded a large grain of the β phase [Fig. 11(b)], surrounded by fine grains of the λ phase. This transformation occurred abruptly between about 1220 and 1240 K (but there is considerable uncertainty in the exact temperature—see Sec. II). It can be seen that the (110) reflections of the β phase show good lattice match with the fivefold axes of the icosahedral phase. Also note that the spatial orientation of one of the (110) reflections corresponds to one of the twofold reflections (arrows in Fig. 11). Energy dispersive spectroscopy showed that the β phase was lower in Al than the quasicrystal.

An alternative means of transforming a ccp cluster into an ip cluster, while retaining a close relationship among some high-symmetry axes, was described by Mackay.[45] The result is shown in Fig. 12. In Mackay's transformation, the threefold axis remains parallel in both ccp and ip structures, but rotates by 37.8°. This is equivalent to rotating the stereographic projection in Fig. 8(a) clockwise by 37.8°, and it serves the purpose of aligning the other three threefold axes of ccp with three of the threefold axes of ip. Also, the ccp fourfold axes align with some of the ip twofold axes. The ccp [211]-type axes come within 7.8° of other ip twofold axes. These alignments, shown in Figs. 12(a) and 12(b), have been observed experimentally in at least three systems.[46–48]

However, the Mackay transformation is not consistent with the experimental data. First, the 37.8° rotation of the threefold axis should be easily visible by comparing Figs. 1(c) and 1(d), but it is not present. Second, the diffraction pattern of the overlayer on the twofold icosahedral surface should have fourfold symmetry, rather than the observed twofold symmetry (Fig. 4). Finally, the ip fivefold axis would come closest to the [210]-type ccp axis (5.2° off). The (210) surface would have a rectangular unit cell, as observed. Five equivalent threefold axes would surround the fivefold axes, also consistent with the observation of five rectangular domains on the fivefold surfaces. However, the edge lengths of the rectangles would be in the ratio 2.24, far from the observed ratio of 1.4. Hence, the experimental data for all three surfaces are much more consistent with the transformation shown in Figs. 7 and 9.

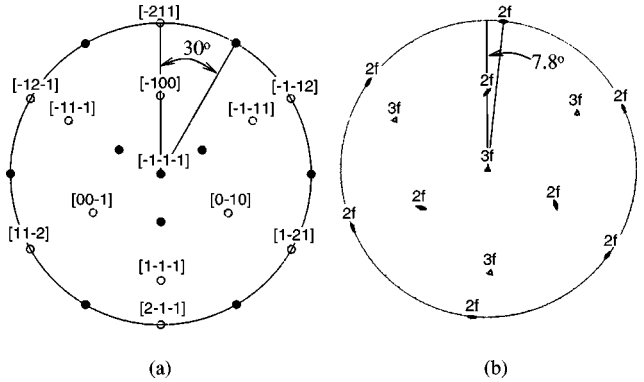

FIG. 12. Stereographic projection of (a) cubic [111] zone axis; (b) icosahedral threefold zone axis. The azimuthal relationship between the two projections is that proposed by Mackay. The high-symmetry axes that are parallel, or nearly so, in the two structures are labeled.

Note that the above discussion is based on the symmetry relationships between cubic and icosahedral systems, and not on details of atomic arrangements within those systems. In reality, we are dealing with binary or ternary systems, with two or three different atomic radii, instead of equally sized spheres. The atomic structure of icosahedral quasicrystals is so complicated that there is no universally accepted structure model in existence thus far. However, all cubic structures have symmetries similar to ccp and all icosahedral quasicrystals have the same symmetry as ip. Hence, the simple model presented in Fig. 7(a) is not too unrealistic. In fact, its ability to explain our experimental data suggests that it is quite plausible.

IV. DISCUSSION

Overlayers of the cubic CsCl structure can be produced on surfaces of quasicrystals by ion sputtering and annealing to temperatures below ~700 K. The CsCl overlayers are deeper than about five atomic layers, because they obscure the diffraction spots from the underlying quasicrystalline substrate.

The low-temperature phases are metastable. They transform irreversibly to the quasicrystalline(like) patterns above ~700 K. Presumably, the low-temperature annealing serves to activate surface and near-surface diffusion, allowing localized rearrangement. However, the temperature is too low to allow long-range diffusion to/from the bulk, so the composition of the surface and near-surface region remains off-stoichiometry. At higher temperatures, the surface composition is restored by equilibration with the bulk, leading to the LEED patterns that we assign to a quasicrystal or high-order approximant. A similar phenomenon has been found in the crystalline FeAl system.[49] After sputtering and subsequent annealing to about 670 K, the FeAl (100) surface formed an Al-deficient phase, Fe_3Al. After annealing at or above 870 K a well-ordered FeAl(100) surface was reestablished. Kottcke *et al.*[49] postulated that this was driven by sputtering-induced changes in surface composition.

The LEED data indicate that the low-temperature structures that form on two chemically different, but symmetrically equivalent quasicrystal samples—fivefold Al-Cu-Fe and fivefold Al-Pd-Mn—are the same. This indicates that the results have some level of generality among different alloys. Furthermore, a series of patterns is observed on chemically identical, but symmetrically inequivalent surfaces (twofold, threefold, and fivefold Al-Pd-Mn). This series can be under-

stood within a general framework based upon the related symmetries of ccp and ip materials. Our model explains not only the symmetries of the surface terminations of the CsCl overlayers, but also the number and orientations of domains.

The threefold surface presents several exceptions to these generalizations. First, not one but two distinguishable patterns are present in the temperature range below 700 K. The first, the facetted pattern, is not assigned to a real-space model at present. It is different from the other low-temperature patterns in that it is visible immediately after sputtering, without annealing (although this effect is not unprecedented[50,51]). The second pattern contains distinctive streaks that may arise from domain structure. The detailed nature of the crystalline overlayers on the threefold surface requires further investigation. However, these unresolved issues should not obscure the fundamental observations: The data support the assignment of the streaked pattern as the CsCl phase, and are consistent with the model for the symmetry relationship given in Figs. 8 and 9. Hence, the streaked pattern falls within the framework described above.

ACKNOWLEDGMENTS

Michel Van Hove, Tanja Drobek, and Jean Marie Dubois provided valuable comments and suggestions. We also wish to acknowledge that three other groups (led by J. Chevrier, L. Schlapbach, and M. Erbudak) have been working in parallel with us, studying cubic overlayers on quasicrystalline substrates. We especially thank D. Naumović from one of those groups, for sharing results and ideas. This work was supported by the Director, Office of Energy Research, Office of Basic Energy Sciences, Materials Sciences Division, of the U.S. Department of Energy under Contract No. W-405-Eng-82.

*Author to whom correspondence should be addressed. FAX: 515-294-4709. Electronic address: thiel@ameslab.gov

[1] D. Shechtman, I. Blech, D. Gratias, and J. W. Cahn, Phys. Rev. Lett. **53**, 1951 (1984).

[2] D. Shechtman and I. Blech, Metall. Trans. A **16**, 1005 (1985).

[3] A. I. Goldman and M. Widom, Annu. Rev. Phys. Chem. **42**, 685 (1991).

[4] P. W. Stephens and A. I. Goldman, Sci. Am. **264**, (4) 24 (1991).

[5] C. Janot, *Quasicrystals: A Primer*, edited by C. J. Humphreys, P. B. Hirsch, N. F. Mott, and R. J. Brook, Monographs on the Physics and Chemistry of Materials (Clarendon, Oxford, 1992).

[6] A. I. Goldman and K. F. Kelton, Rev. Mod. Phys. **65**, 213 (1993).

[7] J. M. Dubois and P. Weinland, European Patent No. EP 0356287 A1 and U.S. Patent No. 5204191 (20 April 1993).

[8] J. M. Dubois, in *Introduction to the Structure, Physical Properties and Appplications of Quasicrystalline Alloys*, edited by J. B. Suck, M. Schreiber, and P. Hausler (Springer-Verlag, Berlin, in press).

[9] R. G. Musket, W. McLean, C. A. Colmenares, D. M. Makowiecki, and W. J. Siekhaus, Appl. Surf. Sci. **10**, 143 (1982).

[10] P. Ebert, S. Yue, and K. Urban, Phys. Rev. B **57**, 2821 (1998).

[11] C. Janot and M. de Boissieu, Phys. Rev. Lett. **72**, 1674 (1994).

[12] C. Janot, Phys. Rev. B **53**, 181 (1996).

[13] C. Janot and J.-M. Dubois, in *Introduction to Structure, Physical Properties and Application of Quasicrystalline Alloys*, edited by J. B. Suck, M. Schreiber, and P. Hausler (Springer-Verlag, Berlin, in press).

[14] T. M. Schaub, D. E. Bürgler, H.-J. Güntherodt, J. B. Suck, and M. Audier, Appl. Phys. A: Mater. Sci. Process. **61**, 491 (1995).

[15] S.-L. Chang, W. B. Chin, C.-M. Zhang, C. J. Jenks, and P. A. Thiel, Surf. Sci. **337**, 135 (1995).

[16] S.-L. Chang, J. W. Anderegg, and P. A. Thiel, J. Non-Cryst. Solids **195**, 95 (1996).

[17] S. Suzuki, Y. Waseda, N. Tamura, and K. Urban, Scr. Mater. **35**, 891 (1996).

[18] D. Naumović, P. Aebi, L. Schlapbach, C. Beeli, T. A. Lograsso, and D. W. Delaney, in *Proceedings of the Sixth International Conference on Quasicrystals (ICQ6)*, edited by T. Fujiwara, and S. Takeuchi (World Scientific, Singapore, 1998), pp. 749–756.

[19] D. Rouxel, M. Gavatz, P. Pigeat, B. Weber, and P. Plaindoux, in *Proceedings of the Conference, ''New Horizons in Quasicrystals: Research and Applications,''* edited by A. I. Goldman, D. Sordelet, P. A. Thiel, and J. M. Dubois (World Scientific, Singapore, 1997), pp. 173–180.

[20] Z. Shen, P. J. Pinhero, T. A. Lograsso, D. W. Delaney, C. J. Jenks, and P. A. Thiel, Surf. Sci. **385**, L923 (1997).

[21] M. Zurkirch, M. Erbudak, and A. R. Kortan, in *Proceedings of the Sixth International Conference on Quasicrystals (ICQ6)* (Ref. 18), pp. 67–70.

[22] D. Naumović (unpublished).

[23] Z. Zhang, Y. C. Feng, D. B. Williams, and K. H. Kuo, Philos. Mag. B **67**, 237 (1993).

[24] Z. Wang, X. Yang, and R. Wang, J. Phys.: Condens. Matter **5**, 7569 (1993).

[25] R. Wang, X. Yang, H. Takahashi, and S. Ohnuki, J. Phys.: Condens. Matter **7**, 2105 (1995).

[26] X. Yang, R. Wang, and X. Fan, Philos. Mag. Lett. **73**, 121 (1996).

[27] W. Liu, M. Schmücker, and U. Köster, Phys. Status Solidi A **124**, 75 (1991)

[28] C. Dong, J. M. Dubois, S. S. Kang, and M. Audier, Philos. Mag. B **65**, 107 (1992).

[29] C. Dong, K. Chattopadhyay, and K. H. Kuo, Scr. Metall. **21**, 1307 (1987).

[30] C. Dong, K. H. Kuo, and K. Chattopadhyay, Mater. Sci. Forum **22-24**, 555 (1987).

[31] C. Dong and J. M. Dubois, J. Non-Cryst. Solids **159**, 107 (1993).

[32] C. J. Jenks, P. J. Pinhero, Z. Shen, T. A. Lograsso, D. W. Delaney, T. E. Bloomer, S.-L. Chang, C.-M. Zhang, J. W. Anderegg, A. H. M. Z. Islam, A. I. Goldman, and P. A. Thiel, in *Proceedings of the Sixth International Conference on Quasicrystals (ICQ6)* (Ref. 18), pp. 741–748.

[33] L. E. Davis, N. C. MacDonald, P. W. Palmberg, G. E. Riach, and R. E. Weber, *Handbook of Auger Electron Spectroscopy* (Physical Electronics Division, Perkin-Elmer Corporation, Eden Prairie, MN, 1978).

[34] W. Raberg, Ph.D. Thesis, Universität Bonn, 1998.

[35] J. Chevrier, G. Cappello, F. Comin, and J. P. Palmari, in *Proceedings of the Conference, ''New Horizons in Quasicrystals: Research and Applications''* (Ref. 19), pp. 144–151.

[36] Z. Shen, W. Raberg, M. Heinzig, C. J. Jenks, T. Lograsso, D. Delaney, and P. A. Thiel (unpublished).

[37] F. Shi, Z. Shen, D. W. Delaney, A. I. Goldman, C. J. Jenks, M. J. Kramer, T. Lograsso, P. A. Thiel, and M. A. Van Hove, Surf. Sci. **411**, 86 (1998).

[38] A. J. Bradley and H. J. Goldschmidt, J. Inst. Met. **65**, 389 (1939).
[39] P. Villars and L. D. Calvert, *Pearson's Handbook of Crystallographic Data for Intermetallic Phases* (ASM International, Materials Park, OH, 1991), Vol. 1.
[40] M. Henzler, Surf. Sci. **22**, 12 (1970).
[41] D. K. Flynn, W. Wang, S.-L. Chang, M. C. Tringides, and P. A. Thiel, Langmuir **4**, 1096 (1988).
[42] C. J. Jenks, S.-L. Chang, J. W. Anderegg, P. A. Thiel, and D. W. Lynch, Phys. Rev. B **54**, 6301 (1996).
[43] Z. Shen, C. J. Jenks, J. W. Anderegg, D. W. Delaney, T. A. Lograsso, P. A. Thiel, and A. I. Goldman, Phys. Rev. Lett. **78**, 1050 (1997).
[44] For instance, in the previous *in situ* high-energy irradiation studies by Wang and co-workers (Refs. 24–26), the electron transparent region was fully penetrated by the Ar ions. This disrupted the quasicrystal through the full thickness of the analyzed region, not just at the surface, as in this study. Hence, the crystallographic relationships derived from the previous work are more tenuous since the β phase probably nucleated tens of micrometer away from the remaining quasicrystalline region, not nanometers away as in this study.
[45] A. L. Mackay, Acta Crystallogr. **15**, 916 (1962).
[46] D. C. Koskenmaki, H. S. Chen, and K. V. Rao, Phys. Rev. B **33**, 5328 (1986).
[47] M. Audier, P. Sainfort, and B. Dubost, Philos. Mag. B **54**, L105 (1986).
[48] X. Zhang and K. F. Kelton, Philos. Mag. Lett. **63**, 39 (1991).
[49] M. Kottcke, H. Graupner, D. M. Zehner, L. Hammer, and K. Heinz, Phys. Rev. B **54**, R5275 (1996).
[50] D. Naumović (private communication).
[51] M. Heinzig [unpublished results for the (110) surface of bulk Al-Pd-Mn].